Superionic Conductors

Deutsche Ausgabe: DOI: 10.1002/ange.201601546
Internationale Ausgabe: DOI: 10.1002/anie.201601546

An Air-Stable Na_3SbS_4 Superionic Conductor Prepared by a Rapid and Economic Synthetic Procedure

*Hui Wang, Yan Chen, Zachary D. Hood, Gayatri Sahu, Amaresh Samuthira Pandian, Jong Kahk Keum, Ke An, and Chengdu Liang**

Abstract: *All-solid-state sodium batteries, using solid electrolyte and abundant sodium resources, show great promise for safe, low-cost, and large-scale energy storage applications. The exploration of novel solid electrolytes is critical for the room temperature operation of all-solid-state Na batteries. An ideal solid electrolyte must have high ionic conductivity, hold outstanding chemical and electrochemical stability, and employ low-cost synthetic methods. Achieving the combination of these properties is a grand challenge for the synthesis of sulfide-based solid electrolytes. Design of the solid electrolyte Na_3SbS_4 is described, realizing excellent air stability and an economic synthesis based on hard and soft acid and base (HSAB) theory. This new solid electrolyte also exhibits a remarkably high ionic conductivity of 1 mS cm^{-1} at 25 °C and ideal compatibility with a metallic sodium anode.*

Rechargeable sodium (Na) batteries show great promise for large-scale energy storage systems[1–3] (such as, electric vehicles and grids) as a result of the high abundance and low cost of sodium. To meet both safety and efficiency concerns, room temperature operation is highly desirable for all-solid-state Na batteries. To realize this target, solid electrolytes are of critical importance. An ideal solid electrolyte must have high ionic conductivity, hold good chemical stability under ambient conditions, and employ a low-cost synthetic method. The promising higher ionic conductivities of sulfide-based electrolytes[4–6] (for example, Na_3PS_4, Na_4SiS_4, and $Na_{10}GeP_2S_{12}$) compared with classical sodium super ionic conductor (NASICON) compounds[7–9] (for example, $Na_{1+x}Zr_3P_{3-x}Si_xO_{12}$), has led to a gain in popularity of the former. For example, Hayashi and co-workers[4] reported a glass-ceramic Na_3PS_4 with an ionic conductivity of 2×10^{-4} S cm^{-1}; $Na_{10}GeP_2S_{12}$ was predicted to have an ionic conductivity as high as 4.7×10^{-4} S cm^{-1} based on a first-principles simulation.[6] Despite the scientific importance of these results, sulfide-based solid electrolytes still face a huge challenge, which is the fact that most of these materials are air- or moisture-sensitive. When exposed to an ambient environment, they are rapidly hydrolyzed, leading to release of noxious H_2S gas and a tremendous decrease in the ionic conductivity of the solid electrolyte. The stability of the sulfide closely follows hard and soft acid and base (HSAB) theory, where a hard acid reacts preferentially with a hard base and a soft acid is prone to reacting with a soft base. For instance, most thiophosphate-themed superionic conductors are not stable in air because oxygen is a hard base that reacts preferentially with phosphorus (the hard acid) and replaces sulfur (the soft base).[10] To overcome this limitation, we revisited Group VA elements on the periodic table to search for appropriate soft acids that will bind strongly with sulfur.

Based on HSAB theory, we determined that $Na_3SbS_4\cdot9H_2O$ (also known as Schlippe's salt) is a promising candidate. This salt is available in nature, which suggests that the $(SbS_4)^{3-}$ group should be stable in an ambient atmosphere because of the strong bonding between the soft acid (Sb^{5+}) and the soft base (S^{2-}). Furthermore, this stability could allow for low temperature heat treatment as a straightforward synthetic route to remove crystalline water and produce Na_3SbS_4, without chemical decomposition. Thus, we speculated that it might be possible to use Na_3SbS_4 as a stable solid electrolyte in an ambient environment. Herein, we report the rapid synthesis, outstanding ionic conductivity, and mechanism of Na^+ conduction for the Na_3SbS_4 solid electrolyte. We also demonstrate that this new solid electrolyte shows superior air stability and good compatibility with a metallic sodium anode.

$Na_3SbS_4\cdot9H_2O$, is a commercial precursor salt from which antimony pentasulfide (Sb_2S_5) may be prepared.[11] When heated, $Na_3SbS_4\cdot9H_2O$ loses the water complexed with the salt, and thus forms a pure phase of Na_3SbS_4. Thermogravimetric analysis (TGA) allowed us to trace the removal of water from $Na_3SbS_4\cdot9H_2O$. The TGA curve in Figure 1a shows two steps, with a large weight loss before 100 °C (ca. 30 %) and a second smaller step around 175 °C (3.5 %). These two distinct weight deviation peaks arise from a step-by-step dehydration process, which is associated with different types of hydrogen bonding (H-O-H and H-O-S).[11,12] No further obvious weight loss was observed until 300 °C was reached. The water removal process from $Na_3SbS_4\cdot9H_2O$ was also monitored by in situ powder *x*-ray diffraction (XRD). At room temperature (25 °C), $Na_3SbS_4\cdot9H_2O$ exhibits a cubic phase and complicated diffraction patterns (Figure 1b).

[*] Dr. H. Wang, Z. D. Hood, Dr. G. Sahu, Dr. A. S. Pandian, Dr. J. K. Keum, Dr. C. D. Liang
Center for Nanophase Materials Sciences
Oak Ridge National Laboratory
Oak Ridge, TN 37831 (USA)
E-mail: cd_liang@hotmail.com
Dr. Y. Chen, Dr. J. K. Keum, Dr. K. An
Chemical and Engineering Materials Division
Oak Ridge National Laboratory
Oak Ridge, TN 37831 (USA)
Z. D. Hood
School of Chemistry and Biochemistry
Georgia Institute of Technology
Atlanta, GA 30332 (USA)

Supporting information for this article can be found under: http://dx.doi.org/10.1002/anie.201601546.

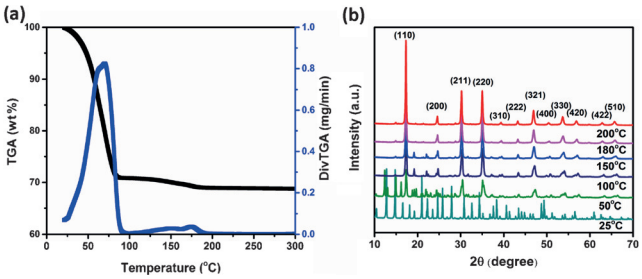

Figure 1. a) TGA of $Na_3SbS_4{\cdot}9H_2O$. TGA curve (black line), deviation of weight loss from room temperature to 300 °C under N_2 (blue line); b) In situ XRD patterns of $Na_3SbS_4{\cdot}9H_2O$ with increasing temperature (25–200 °C) under N_2.

With increasing temperature, peaks at $2\theta = 10.5$, 12.9, and 16.6° become weaker and disappear at 100 °C, while the peaks located at $2\theta = 21.1$ and 22.3° are stable up to higher temperatures. The variation of XRD patterns clearly reveals two steps associated with elimination of water from $Na_3SbS_4{\cdot}9H_2O$, which is consistent with TGA. When the temperature reaches 180 °C, a pure Na_3SbS_4 cubic phase forms with characteristic peaks at $2\theta = 17.3$, 30.2, 35.1, and 47.1°, corresponding to (110), (211), (220), and (321) planes, respectively. High-temperature XRD patterns (Supporting Information, Figure S1) provide strong evidence for the stability of the Na_3SbS_4 cubic phase at 300 °C. Upon cooling to room temperature, Na_3SbS_4 exhibits a slight structural distortion from the cubic phase to the tetragonal phase (Supporting Information, Figure S1).[13] SEM images indicate that Na_3SbS_4 possesses a highly porous morphology in comparison with dense $Na_3SbS_4{\cdot}9H_2O$ (Supporting Information, Figure S2).

The ionic conductivity of $Na_3SbS_4{\cdot}9H_2O$ samples was determined after heat treatment at different temperatures (25–180 °C) under vacuum. Figure 2a displays typical Arrhenius plots for the original $Na_3SbS_4{\cdot}9H_2O$ and as-synthesized Na_3SbS_4 in the range of 25–100 °C. Figure 2b presents the room temperature ionic conductivity (left *y*-axis) and activation energy (right *y*-axis) versus the heat treatment temperature. The conductivity was calculated from the electrochemical impedance spectra (EIS; Supporting Information, Figure S3).

Pristine $Na_3SbS_4{\cdot}9H_2O$ has a poor ionic conductivity of 5×10^{-7} S cm^{-1} at room temperature. After removing H_2O, the

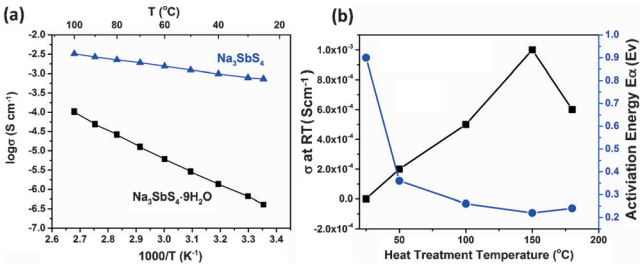

Figure 2. a) Arrhenius plots of $Na_3SbS_4{\cdot}9H_2O$ and Na_3SbS_4. b) Room temperature ionic conductivity (left *y*-axis) and activation energies (right *y*-axis) versus the temperature of heat treatment.
Key: conductivity (—■—), activation energy (—●—).

room temperature (25 °C) ionic conductivity of this material dramatically increased and reached a maximum after heating of the complex at 150 °C under vacuum. The XRD pattern confirms that this sample is the pure Na_3SbS_4 phase (Supporting Information, Figure S4), indicating that 150 °C heat treatment is adequate to remove waters of hydration under vacuum. The ionic conductivity of the pure Na_3SbS_4 phase is at its highest (1.05 mS cm^{-1}) at room temperature, nearly four orders of magnitude higher than that of $Na_3SbS_4{\cdot}9H_2O$, and is obviously more conductive than sulfide-based glass-ceramics[4,14,15] and $Na_3Zr_2Si_2PO_{12}$ crystals.[8] Moreover, this solid electrolyte shows a comparable ionic conductivity with that of Na_3PSe_4[16] (the best chalcogenide Na-ion conductor) but requires a much simpler synthetic route. The electronic conductivity of Na_3SbS_4 was determined by DC polarization measurement, which gave a value of 1.9×10^{-10} S cm^{-1}. Additionally, the activation energy versus the temperature of heat treatment displayed an inverted peak in conductivity (Figure 2b). The lowest activation energy was observed for the sample treated at 150 °C; this material also had the highest ionic conductivity. The activation energy was as low as 0.22 eV when compared to other well-known Na solid electrolytes.[4] Such a low activation energy value ensures a flat conductivity curve over a broad temperature range.

The striking difference in ionic conductivity between $Na_3SbS_4{\cdot}9H_2O$ and Na_3SbS_4 results from structural differences. The crystal structure of pristine $Na_3SbS_4{\cdot}9H_2O$ (Supporting Information, Figure S5) lacks connective tunnels for Na^+ transport, thus exhibiting a lower ionic conductivity. In contrast, the Na_3SbS_4 framework contains accessible and connected tunnels. Thanks to the advantages of neutron diffraction (such as differential element scattering contrasts), the tetragonal crystal structure ($P\bar{4}2_1c$ space group) and subtle structural information such as site occupancies (Figure 3; Supporting Information, Table S1) have been revealed for Na_3SbS_4. Neutron diffraction measurements were performed at the VULCAN diffractometer (SNS at ORNL). The possible Na^+ transport tunnels are visualized in Figure 3b,c with the aid of the structure model. There are two main sites for Na atoms in the Na_3SbS_4 lattice: Na(1) in a NaS_6 distorted octahedron, and Na(2) in a NaS_8 dodecahedron. In the *xy*-plane (Figure 3b), the NaS_6 and NaS_8 sites are alternatively arranged and are connected by shared faces. An infinite planar tunnel network, -Na(1)-Na(2)-Na(1)-Na(2)-, forms to enable Na^+ transport through the Na_3SbS_4 framework. Moreover, the NaS_6 octahedra are mutually linked with shared edges along the *z*-axis (Figure 3c), which allows Na^+ to hop across the planar network. Therefore, a 3D tunnel network is constructed by the combination of a planar pathway and an interplane chain pathway in the Na_3SbS_4 framework. These accessible tunnels in the lattice enable fast ion transport in the solid electrolytes.[16,20] The proposed conductive mechanism is supported by the anisotropic atomic displacement parameters (U_{ij}) in Table S1 (Supporting Information). The disk-like Na(2) ellipsoid shows a preferential vibration direction toward the four neighboring Na(1) sites, and less so toward the Sb sites, supporting the proposed planar pathway in the *xy*-plane. Similarly, the Na(1) ellipsoid is more likely to connect Na(2) sites in the *xy*-plane and the

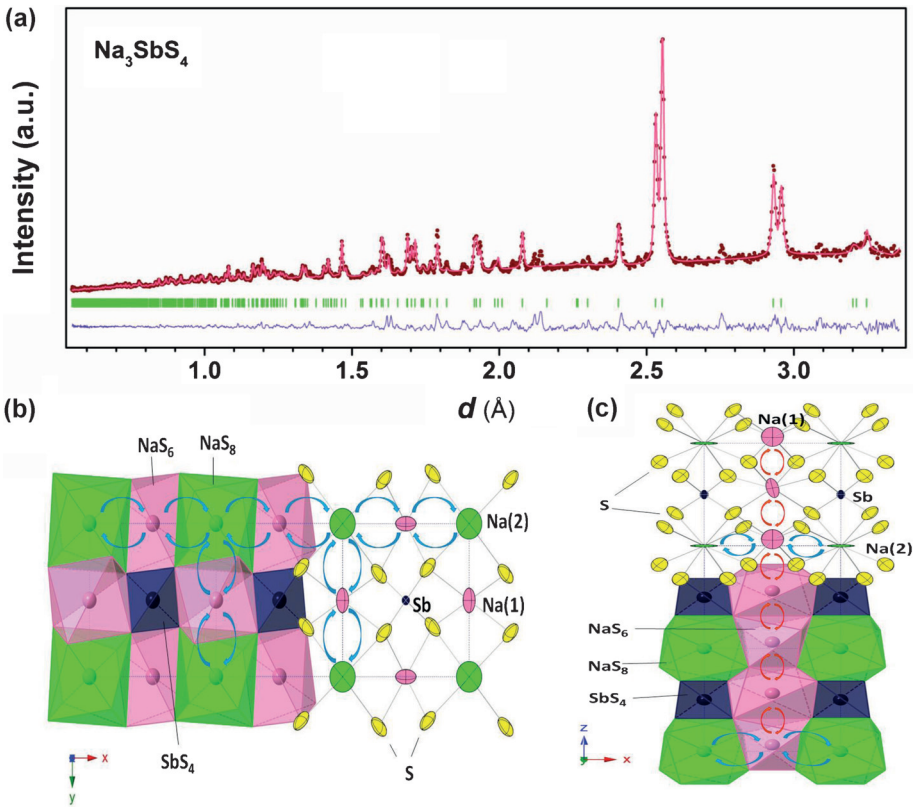

Figure 3. a) Neutron diffraction pattern and Rietveld refinement of Na_3SbS_4 at room temperature. b) [001] and c) [010] views of the framework structure of Na_3SbS_4. The 2D planar Na^+ transport tunnels in the *xy*-plane are formed by alternatively arranged NaS_6 and NaS_8 polyhedra, which share common faces. Planar tunnels are connected along the *z*-axis through chains formed by NaS_6 octahedra, which share common edges.

neighboring Na(1) sites along the *z*-axis, thereby forming the interplane chain pathway. Furthermore, within the tunnel, the Na(2) site is characterized by a 5% vacancy, as indicated by Rietveld refinement (Supporting Information, Table S1). The existence of sufficient vacancies is beneficial for Na^+ hopping.[18,21] Additionally, the surface conduction[22] related to the highly porous structure of Na_3SbS_4 also potentially contributes to its high ionic conductivity.

The chemical stability of solid electrolytes under an ambient environment is highly desirable, which allows for easy handling and dramatically reduced production costs. An air-stability experiment was carried out with Na_3SbS_4 by exposing the as-synthesized sample to an ambient atmosphere for 48 h (humidity 70%). Figure 4a compares the Raman spectra of pure Na_3SbS_4 and the air-exposed sample. The characteristic asymmetric (ν_a) and symmetric (ν_s) stretching vibration peaks of the SbS_4 group in Na_3SbS_4 were observed at 410/389 and 368 cm^{-1}, respectively, which is in good agreement with previous reports.[12,13] The air-exposed sample showed a slight shift of the ν_a peak of SbS_4 to 380 cm^{-1}, appearance of a ν_s peak at the same location, as well as a broad absorption hump at 3400 cm^{-1} (corresponding to absorbed H_2O). In fact, the Raman spectrum of the air-exposed sample is consistent with that of $Na_3SbS_4{\cdot}9H_2O$.[12,13] XRD patterns (Figure 4b) present the same diffraction peaks in the air-exposed and $Na_3SbS_4{\cdot}9H_2O$ samples. Hence, both Raman and XRD results confirm the previous predictions based on HSAB theory; namely, that Sb^{5+} soft acid is able to bind strongly with a soft base such as S^{2-}, which allows the Na_3SbS_4 solid electrolyte to retain chemical stability in an ambient environment. This observation is in complete contrast to that for thiophosphates (Li_2S-P_2S_5, Li_3PS_4, and Na_3PS_4),[23–25] which suffer from quick hydrolysis and degradation to their structures when exposed to air. Interestingly, the pure Na_3SbS_4 phase can be restored by heating of the air-exposed sample at 150 °C for 1 h, which is reflected by the equivalence of the Raman spectra and XRD patterns obtained for reheated air-exposed sample and pure Na_3SbS_4. This fact further demonstrates that Sb^{5+} (soft acid) and S^{2-} (soft base) are strongly bonded in Na_3SbS_4, which allows reversible H_2O absorption/desorption. Additionally, air-exposed Na_3SbS_4 in a desiccator (20% humidity) produces XRD patterns that are closely comparable to that of pure Na_3SbS_4 (Supporting Information, Figure S6).

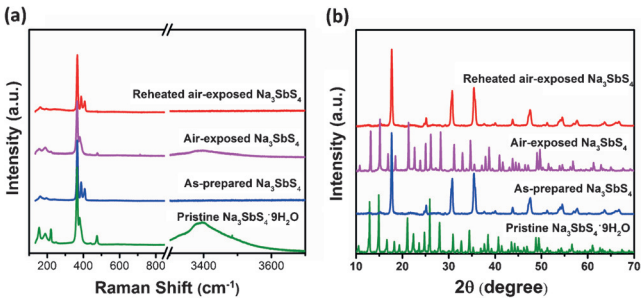

Figure 4. Structural evaluation of Na_3SbS_4 upon air exposure: a) Raman spectra and b) XRD patterns of pristine $Na_3SbS_4{\cdot}9H_2O$, as-synthesized Na_3SbS_4, air-exposed Na_3SbS_4 (48 h), and reheated air-exposed Na_3SbS_4 sample (150 °C for 1 h under vacuum).

Besides the structural variations described above, we also measured the ionic conductivity of the pure Na_3SbS_4 and reheated air-exposed sample. Typical Arrhenius plots (temperature dependent) are presented in Figure S7 (Supporting Information). The room temperature ionic conductivity of the reheated sample was 0.9 mS cm^{-1}, indicating that superior ionic conductivity is maintained.

The electrochemical compatibility of Na_3SbS_4 against a metallic Na anode was evaluated with Na/Na_3SbS_4/Na symmetric cells. These symmetric cells are composed of

a pressed Na_3SbS_4 pellet between two metallic Na foils inside Swagelok cells. The voltage profile demonstrates great cyclability of Na_3SbS_4 and the metallic Na anode (Figure 5a), unlike other discovered sulfide-based solid electrolytes with

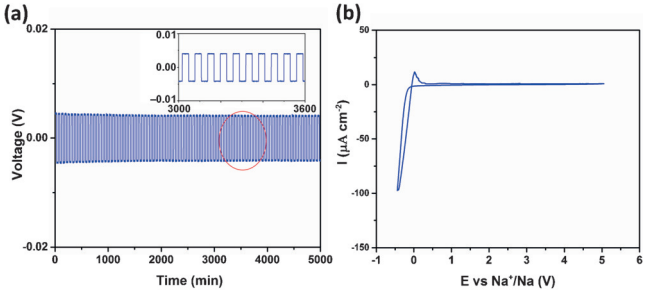

Figure 5. a) Cyclability of Na_3SbS_4 in a symmetric $Na/Na_3SbS_4/Na$ cell with a current density of 0.1 $mA\,cm^{-2}$ at room temperature; b) a representative CV of a $Na/Na_3SbS_4/Pt$ cell vs. Na/Na^+; from −0.5 to 5.0 V at a scan rate of 5 $mV\,s^{-1}$.

Ge or Sn as dopants.[26,27] Given the high valence of Sb^{5+}, good electrochemical compatibility is associated with formation of the solid electrolyte interphase (SEI). The SEI formed between solid electrolyte and anode can effectively stabilize the interface and prevent further interfacial reactions.[28,29] Furthermore, the electrochemical stability of Na_3SbS_4 and metallic Na was investigated with cyclic voltammetry (CV) measurements of a $Na/Na_3SbS_4/Pt$ cell. As shown in the CV curve (Figure 5b), the cathode current corresponding to Na deposition started just below 0 V, while the anodic current associated with sodium dissolution showed a peak between 0 and 0.5 V. No significant current was observed in the potential range of 0.5–5 V, which confirms that Na_3SbS_4 solid electrolyte is electrochemically stable in conjunction with metallic Na, and that no adverse side reactions occur over a wide voltage window.

In summary, we report a novel Na_3SbS_4 superionic conductor as a solid electrolyte for all-solid-state Na batteries. On the basis of HSAB theory, Na_3SbS_4 shows excellent chemical stability under ambient conditions and requires a simple synthetic route. This new solid electrolyte also holds a remarkable ionic conductivity of 1 $mS\,cm^{-1}$ as a result of 3D tunnels provided by its framework, which are available for fast Na^+ transport. The electrochemical stability of Na_3SbS_4 with a metallic Na anode was also demonstrated. This work provides unique insight into current state-of-the-art methods for preparing solid electrolytes and also indicates that HSAB theory may guide the design of superionic conductors toward materials with improved air stability. The application of HSAB in the design of solid electrolytes will have a far-reaching impact on the development of high-energy all-solid-state batteries.

Acknowledgements

The synthesis and characterization portions of the research (H.W., A.S.P., J.K.K., Z.D.H.) were supported by the Center for Nanophase Materials Sciences in Oak Ridge National Laboratory (ORNL), which is a U.S. Department of Energy (DOE) office of Science User Facility. The theory and neutron scattering portions of the research (Y.C., G.S., K.A., C.L.) were sponsored by the Division of Materials Sciences and Engineering, Office of Basic Energy Sciences, U.S. DOE. A portion of the research was carried out as a user project at the Spallation Neutron Source at ORNL, which is sponsored by the Scientific User Facilities Division, Office of Basic Energy Sciences, U.S. DOE. Z.D.H. gratefully acknowledges the National Science Foundation for a Graduate Research Fellowship under Grant No. DGE-1148903 and the Georgia Tech-ORNL Fellowship. The authors thank Dr. Rui Peng and Dr. Zili Wu for their help with the Raman measurement.

Keywords: air-stable materials · hard and soft acid and base theory (HSAB) · ionic conductivity · solid-state sodium batteries · synthesis

How to cite: *Angew. Chem. Int. Ed.* **2016**, *55*, 8551–8555
Angew. Chem. **2016**, *128*, 8693–8697

[1] J. Liu, J. G. Zhang, Z. G. Yang, J. P. Lemmon, C. Imhoff, G. L. Graff, L. Y. Li, J. Z. Hu, C. M. Wang, J. Xiao, G. Xia, V. V. Viswanathan, S. Baskaran, V. Sprenkle, X. L. Li, Y. Y. Shao, B. Schwenzer, *Adv. Funct. Mater.* **2013**, *23*, 929–946.
[2] H. L. Pan, Y. S. Hu, L. Q. Chen, *Energy Environ. Sci.* **2013**, *6*, 2338–2360.
[3] K. B. Hueso, M. Armand, T. Rojo, *Energy Environ. Sci.* **2013**, *6*, 734–749.
[4] A. Hayashi, K. Noi, A. Sakuda, M. Tatsumisago, *Nat. Commun.* **2012**, *3*, 856.
[5] N. Tanibata, K. Noi, A. Hayashi, M. Tatsumisago, *RSC Adv.* **2014**, *4*, 17120–17123.
[6] V. S. Kandagal, M. D. Bharadwaj, U. V. Waghmare, *J. Mater. Chem. A* **2015**, *3*, 12992–12999.
[7] J. B. Goodenough, H. Y. P. Hong, J. A. Kafalas, *Mater. Res. Bull.* **1976**, *11*, 203–220.
[8] O. Bohnke, S. Ronchetti, D. Mazza, *Solid State Ionics* **1999**, *122*, 127–136.
[9] F. Lalère, J. B. Leriche, M. Courty, S. Boulineau, V. Viallet, C. Masquelier, V. Seznec, *J. Power Sources* **2014**, *247*, 975–980.
[10] G. Sahu, Z. Lin, J. C. Li, Z. C. Liu, N. Dudney, C. D. Liang, *Energy Environ. Sci.* **2014**, *7*, 1053–1058.
[11] K. Mereiter, A. Preisinger, H. Guth, *Acta Crystallogr. Sect. B* **1979**, *35*, 19–25.
[12] K. Mereiter, A. Preisinger, H. Guth, W. Mikenda, K. Hiebl, *Acta Crystallogr. Sect. A* **1978**, *34*, S294–S294.
[13] W. Mikenda, A. Preisinger, *Spectrochim. Acta Part A* **1980**, *36*, 365–370.
[14] S. Susman, L. Boehm, K. J. Volin, C. J. Delbecq, *Solid State Ionics* **1981**, *5*, 667–670.
[15] W. L. Yao, K. Berg, S. Martin, *J. Non-Cryst. Solids* **2008**, *354*, 2045–2053.
[16] L. Zhang, K. Yang, J. L. Mi, L. Lu, L. R. Zhao, L. M. Wang, Y. M. Li, H. Zeng, *Adv. Energy Mater.* **2015**, *5*, 1501294.
[17] K. An, H. D. Skorpenske, A. D. Stoica, D. Ma, X. L. Wang, E. Cakmak, *Metall Mater. Trans. A* **2011**, *42A*, 95–99.
[18] Y. Chen, E. Rangasamy, C. Liang, K. An, *Chem. Mater.* **2015**, *27*, 5491–5494.
[19] S. W. Wang, Y. Chen, S. M. Fang, L. L. Zhang, M. Tang, K. An, K. S. Brinkman, F. L. Chen, *Chem. Mater.* **2014**, *26*, 2021–2029.

[20] S.-H. Bo, Y. Wang, J. C. Kim, W. D. Richards, G. Ceder, *Chem. Mater.* **2016**, *28*, 252 – 258.
[21] Y. Chen, L. Cai, Z. Liu, C. R. dela Cruz, C. Liang, K. An, *Appl. Phys. Lett.* **2015**, *107*, 013904.
[22] Z. Liu, W. Fu, E. A. Payzant, X. Yu, Z. L. Wu, N. J. Dudney, J. Kiggans, K. L. Hong, A. J. Rondinone, C. D. Liang, *J. Am. Che. Soc.,* **2013**, *135*, 975 – 978.
[23] F. Mizuno, A. Hayashi, K. Tadanaga, M. Tatsumisago, *Adv. Mater.* **2005**, *17*, 918 – 921.
[24] E. Rangasamy, Z. C. Liu, M. Gobet, K. Pilar, G. Sahu, W. Zhou, H. Wu, S. Greenbaum, C. D. Liang, *J. Am. Chem. Soc.* **2015**, *137*, 1384 – 1387.
[25] A. Hayashi, K. Noi, N. Tanibata, M. Nagao, M. Tatsumisago, *J. Power Sources* **2014**, *258*, 420 – 423.
[26] E. E. Jay, M. J. D. Rushton, A. Chroneos, R. W. Grimes, J. A. Kilner, *Phys. Chem. Chem. Phys.* **2015**, *17*, 178 – 183.
[27] N. Kamaya, K. Homma, Y. Yamakawa, M. Hirayama, R. Kanno, M. Yonemura, T. Kamiyama, Y. Kato, S. Hama, K. Kawamoto, A. Mitsui, *Nat. Mater.* **2011**, *10*, 682 – 686.
[28] J. C. Li, C. Ma, M. F. Chi, C. D. Liang, N. J. Dudney, *Adv. Energy Mater.* **2015**, *5*, 1408.
[29] Z. D. Hood, H. Wang, A. Samuthira Pandian, J. K. Keum, C. Liang, *J. Am. Chem. Soc.* **2016**, *138*, 1768 – 1771.

Received: February 12, 2016
Published online: June 1, 2016

